

# DETONATION INITIATION INDUCED BY FLAME IMPLOSION AND SHOCK WAVE FOCUSING

*Qin Yaxin, Yu Junli, Gao Ge*

(National Key Laboratory of Science and Technology on Aero-Engines,  
Beijing University of Aeronautics and Astronautics, Beijing, 100191, P. R. China)

**Abstract:** Computational simulations on structurally different detonation generator are carried out to study the phenomena, the mechanism and the gas dynamics characteristics of flame implosion and shock wave focusing. Two-dimensional axisymmetric and unsteady Navier-Stokes equations are numerically solved and detailed chemical reaction kinetics of hydrogen/air mixture is used. The simulation results show that the laminar flame generated by low energy spark in the jet flame burner is accelerated under the narrow channel, the jet flame impinging on the axis strengthens shock wave and the shock wave enhances flame acceleration. Under the function of multiple shock waves and flame, a number of hot spots appear between the wave and the surface. The spots enlarge rapidly, thus forming an over-drive detonation with high pressure, and then declining to stable detonation. Through calculation and analysis, the length of detonation initiation and stable detonation are obtained, thus providing the useful information for further experimental investigations.

**Key words:** detonation; shock wave focusing; flame implosion; deflagration-to-detonation

**CLC number:** V231.2      **Document code:** A      **Article ID:** 1005-1120(2011)01-0057-09

## INTRODUCTION

Pulse detonation engine (PDE) is an unsteady propulsion device that uses extremely high rate of energy release in repetitive detonation waves to produce thrust. Efficient detonation initiation is a key technique to PDE. There are two methods for the detonation initiation: direct initiation and indirect initiation. The power and energy required in the direct detonation initiation is impractical for most situations, therefore, the detonation initiation is usually indirect via deflagration-to-detonation transition (DDT). Generally, circular orifice plates, wedge obstacles or Shchelkin obstacles are designed in pulse detonation chamber to shorten the distance of DDT. But these obstacles increase total pressure loss, thus leading to low propulsive performance. In the method proposed in Ref. [1], the constant pressure combustion took place firstly, then the jet flow injected into a focusing cavity, the flame im-

pinged, the shock wave focused, and the interaction of shock wave and flame occurred, which induced detonation initiation eventually. That is, the detonation is initiated by strengthening the process of DDT via the shock wave focusing and the flame implosion in a short distance.

The phenomena of shock wave focusing refers to that shock wave has convergence behavior in its propagation direction under certain conditions, which restricts the shock wave front to a narrow area, results in the partial high temperature and the high pressure zone, and finally induces the combustible gas ignition deflagration or the detonation wave. Shock wave focusing is an effective way of energy convergence. The well known way of shock wave focusing is that the shock wave reflection at concave surfaces or wedges causes converging of the flow and produces the local zone with extremely high pressure and temperature<sup>[2-4]</sup>. Another way of shock wave focusing is annular shock wave diffraction, reflec-

tion, and ultimately achieving focusing<sup>[5-6]</sup>. Flame implosion refers to that the ring-like flame collides at the axis and enhances shock wave. Computational simulations on structurally different detonation generator are performed to study the phenomena, the mechanism and the gas dynamics characteristic of shock wave focusing and flame implosion, and to provide theory basis for detonation initiation technology.

## 1 COMPUTATIONAL METHOD AND PHYSICAL MODEL

### 1.1 Computational method

Two-dimensional axisymmetric numerical simulations are carried out by using the realizable turbulence model to solve unsteady Navier-Stokes equations with non-equilibrium wall functions treatment near-wall. The governing equations, including continuity, momentum, energy, and component quality, are listed in Eq. (1). The second-order upwind scheme is selected as the equation discretization scheme, and the pressure-implicit with splitting of operators (PISO) algorithm is used because of its obvious superiority on the transient problem. The precision of PISO algorithm largely depends on the time step, that is, the smaller the time step, the higher the calculation accuracy. In the simulation, the adaptive time stepping method is used, and the minimum time step size is  $1 \times 10^{-9}$  s while the maximum is  $5 \times 10^{-6}$  s. The chemical reaction mechanism for hydrogen-air combustion is based on the Chemkin (Chemical reaction simulation software) model. The model consists of 19 elementary reactions among 9 species (listed in Table 1) and the reactions involving  $N_2$  are neglected.

$$\frac{\partial \mathbf{U}}{\partial t} + \frac{\partial \mathbf{F}}{\partial x} + \frac{\partial \mathbf{G}}{\partial y} = \frac{\partial \mathbf{F}_v}{\partial x} + \frac{\partial \mathbf{G}_v}{\partial y} + \mathbf{R} - \frac{\mathbf{G} - \mathbf{G}_v}{y}$$

$$\text{where } \mathbf{U} = \begin{bmatrix} \rho \\ \rho u \\ \rho v \\ \rho E \\ \rho Y_i \end{bmatrix}, \mathbf{F} = \begin{bmatrix} \rho u \\ \rho u^2 + p \\ \rho uv \\ (\rho E + p)u \\ \rho u Y_i \end{bmatrix},$$

$$\mathbf{G} = \begin{bmatrix} \rho v \\ \rho uv \\ \rho v^2 + p \\ (\rho E + p)v \\ \rho v Y_i \end{bmatrix}, \mathbf{F}_v = \begin{bmatrix} 0 \\ \tau_{xx} \\ \tau_{xy} \\ u\tau_{xx} + v\tau_{xy} + q_x \\ -\rho D_i \frac{\partial Y_i}{\partial x} \end{bmatrix},$$

$$\mathbf{G}_v = \begin{bmatrix} 0 \\ \tau_{xy} \\ \tau_{yy} \\ u\tau_{xy} + v\tau_{yy} + q_y \\ -\rho D_i \frac{\partial Y_i}{\partial y} \end{bmatrix}, \mathbf{R} = \begin{bmatrix} 0 \\ 0 \\ \frac{(p - \tau_{\theta\theta})}{y} \\ 0 \\ R_i \end{bmatrix}.$$

Table 1 H<sub>2</sub>/O<sub>2</sub> reaction mechanism

No.	Elemental reaction	$k_{f,r} = A_r T^{\beta_r} e^{-E_r/RT}$		
		$A_r$	$\beta_r$	$E_r / (\text{J} \cdot \text{mol}^{-1})$
1	H+O <sub>2</sub> =O+OH	$5.10 \times 10^{13}$	-0.82	69 078
2	H <sub>2</sub> +O=H+OH	$1.80 \times 10^7$	1.00	36 945
3	H <sub>2</sub> +OH=H <sub>2</sub> O+H	$1.20 \times 10^6$	1.30	15 188
4	OH+OH=H <sub>2</sub> O+O	$6.00 \times 10^5$	1.30	0
5	H+OH+M=H <sub>2</sub> O+M	$7.50 \times 10^{17}$	-2.60	0
	H <sub>2</sub> O enhanced by	$2.00 \times 10^1$	-	-
6	O <sub>2</sub> +M=O+O+M	$1.90 \times 10^8$	0.50	399 820
7	H <sub>2</sub> +M=H+H+M	$2.20 \times 10^9$	0.50	387 440
	H <sub>2</sub> O enhanced by	$6.00 \times 10^0$	-	-
	H enhanced by	$2.00 \times 10^0$	-	-
	H <sub>2</sub> enhanced by	$3.00 \times 10^0$	-	-
8	H <sub>2</sub> +O <sub>2</sub> =OH+OH	$1.70 \times 10^{10}$	0.00	199 910
9	H+O <sub>2</sub> +M=HO <sub>2</sub> +M	$2.10 \times 10^{12}$	-1.00	0
	H <sub>2</sub> O enhanced by	$2.10 \times 10^1$	-	-
	H <sub>2</sub> enhanced by	$3.30 \times 10^0$	-	-
	O <sub>2</sub> enhanced by	$0.00 \times 10^0$	-	-
	N <sub>2</sub> enhanced by	$0.00 \times 10^0$	-	-
10	H+O <sub>2</sub> +O <sub>2</sub> =HO <sub>2</sub> +O <sub>2</sub>	$6.70 \times 10^{13}$	-1.42	0
11	H+O <sub>2</sub> +N <sub>2</sub> =HO <sub>2</sub> +N <sub>2</sub>	$6.70 \times 10^{13}$	-1.42	0
12	HO <sub>2</sub> +H=H <sub>2</sub> +O <sub>2</sub>	$2.50 \times 10^{10}$	0.00	2 928
13	HO <sub>2</sub> +H=OH+OH	$2.50 \times 10^{11}$	0.00	7 949
14	HO <sub>2</sub> +O=OH+O <sub>2</sub>	$4.80 \times 10^{10}$	0.00	4 184
15	HO <sub>2</sub> +OH=H <sub>2</sub> O+O <sub>2</sub>	$5.00 \times 10^{10}$	0.00	4 184
16	HO <sub>2</sub> +HO <sub>2</sub> =H <sub>2</sub> O <sub>2</sub> +O <sub>2</sub>	$2.00 \times 10^9$	0.00	0
17	H <sub>2</sub> O <sub>2</sub> +M=OH+OH+M	$1.20 \times 10^{14}$	0.00	190 370
18	H <sub>2</sub> O <sub>2</sub> +H=HO <sub>2</sub> +H <sub>2</sub>	$1.70 \times 10^9$	0.00	15 690
19	H <sub>2</sub> O <sub>2</sub> +OH=H <sub>2</sub> O+HO <sub>2</sub>	$1.00 \times 10^{10}$	0.00	7 531

## 1.2 Physical model

Several different models are numerically simulated in this paper, and in the simulation the models are axially symmetric and sketch maps of half of the numerical simulation models are shown in Fig. 1. Fig. 1(a) is a rounded detonative chamber ①, which is used to study the phenomenon of flame implosion; Figs. 1(b-d) are composed of the rounded detonative chamber ①, the shock wave focusing cavity with concave surface ② (in 2-D cases, the concave surface is in an arc shape of 150 mm in diameter), the ring-like jet flame burner ③, and the ignition zone ④. The diameter of detonative chamber is 100 mm, and the length is 800 mm (that is the length sum of shock wave focusing cavity and detonative chamber). The size of ring-like jet flame burner ③ is 10 mm × 100 mm. To overcome the interference at the detonative chamber exit, outside zones are increased in the computational models. The computation grid cell is quadrangle, and the grid size is 1 mm. The adaptive grid technique<sup>[7]</sup> is used, and the grid size is increased gradually at the exit of the detonative chamber.

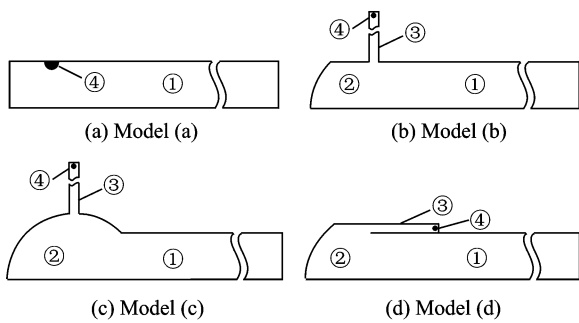


Fig. 1 Sketch maps of numerical simulation model

## 1.3 Initial and boundary conditions

The regions ①, ② and ③ are filled with hydrogen and air. The mixture equivalence ratio is 1.0 and the outside of the detonative chamber is an air domain. The ignition method is hot ignition and the initial pressure and temperature are 0.12 MPa and 1 500 K, respectively in the ignition zone. In other regions the initial pressure and temperature are 0.1 MPa and 300 K. The model bottom is set to be axis boundary, and the right

boundary of the domain is connected to the outside zone. The entire wall is modeled as adiabatic and non-slip.

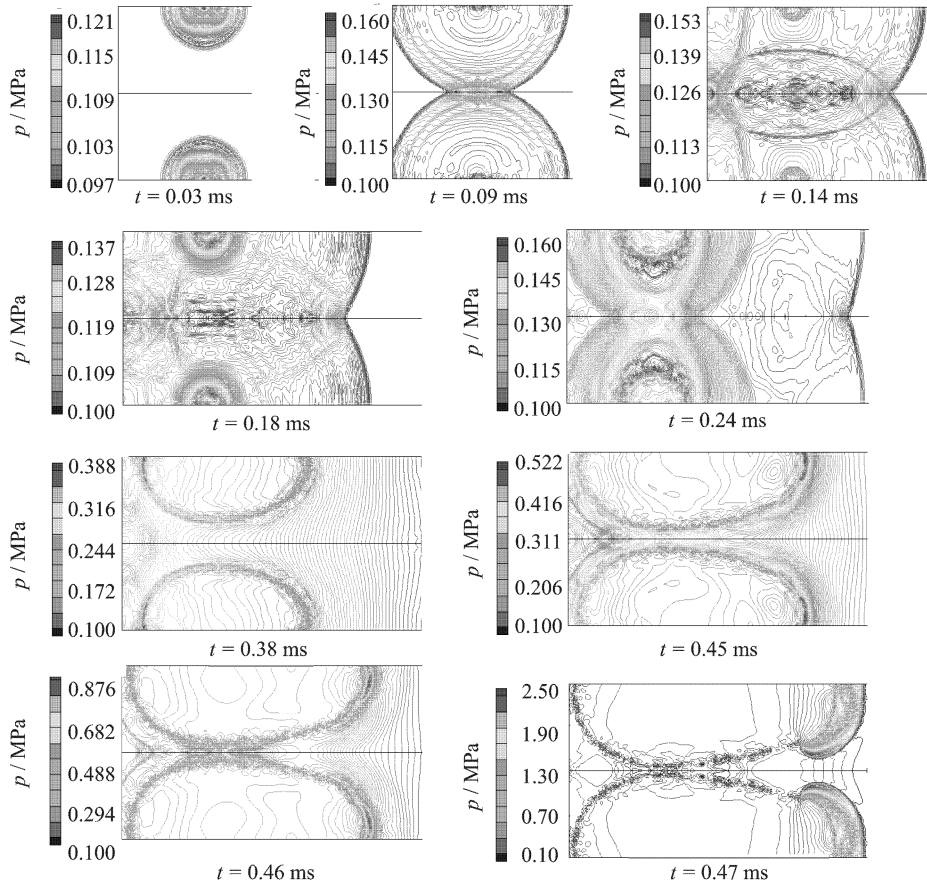
## 2 NUMERICAL RESULTS AND FLOW FIELD ANALYSIS

### 2.1 Flame implosion

The model(a) is simulated to study the phenomenon of flame implosion. Fig. 2 is nephograms of the pressure and the combustion product in a time sequence. Shock wave ahead of flame collides at the axis forms the Mach reflection and the reflected wave propagates to the wall. Mach-stem spreads along the symmetry axis, and the left-spread Mach-stem reflects at the thrust wall. The right-spread Mach-stem continues to decline toward the right side (Fig. 2 (a) ( $t=0.14$  ms)). Flame appears obviously near the wall at  $t=0.18$  ms and the flame shows an ellipse shape due to the restriction of multiple shock waves and axis. The reflected wave from thrust wall confines the left-spread flame speed. However it accelerates the right-spread flame, thus resulting in such a shape of flame forms, as shown in Fig. 2 (b) ( $t=0.45$  ms). The reflected shock wave and the shock wave induced by flame interact and produce the new shock wave gathering to the center (Fig. 2 (a) ( $t=0.38$  ms)). The interaction of shock wave and the right-spread flame of higher speed make the right side shock wave stronger than that on the left side. The right-spread flame speed is higher and the flame gathers at the axis prior to the ignition center, which is flame implosion. Under the interaction of strong shock wave and flame implosion, the over-drive detonation with high pressure forms. The detonation propagates along the axis, and finally declines to stable detonation.

### 2.2 Flame implosion and shock wave focusing

As discussed in the above analyses, the flame implosion benefits the shock wave enhancement, the strong complex shock waves make the flame unstable and accelerated, and the interaction of high-speed flame and strong shock wave promotes



(a) Pressure

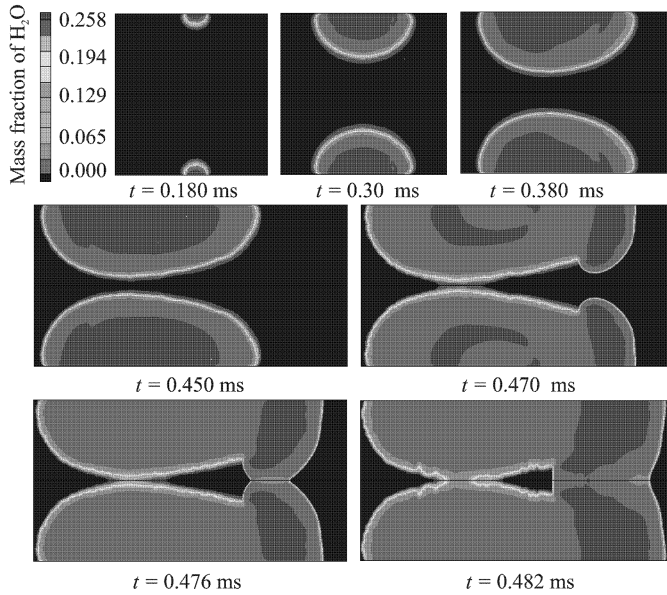
(b) Mass fraction of  $H_2O$ 

Fig. 2 Pressure and combustion product distributions at different time

detonation initiation. Computational simulations on models (b, c) (Fig. 1) reveal that the weak shock wave produced by ignition quickly collides at the axis, as shown in Fig. 3 ( $t=0.217$  ms) and

Fig. 4 ( $t=0.301$  ms) (the distances of flame and shock wave arrive at axis are different in the two models, so the time points are different for the two cases). The laminar flame generated by the

low energy spark in the ring-like jet flame burner is accelerated in narrow channels. The energy released from combustion increases the volume of products. Meanwhile, a series of compression waves come forth, and then merge into the shock wave. The shock wave propagates into the shock wave focusing cavity and the detonative chamber ahead of the flame, and forms a Mach reflection. The Mach-stem spreads along the symmetry axis, as shown in Figs. 3 (a, b) ( $t$  is from 0.284 ms to 0.330 ms), and Figs. 4 (a, b) ( $t$  is from 0.457 ms to 0.484 ms). Then, the flame from the ring-like jet flame burner spreads to the shock wave focusing cavity, expands to all around and converges at the axis. Then shock waves continuously pass through the flame and increase the flame burning rate.

Different shock wave focusing cavities have

different influence on the shock wave and the flame. In the model (b) in Fig. 1, the shock wave induced by flame collides at the axis ahead of flame implosion (Fig. 3 ( $t=0.389$  ms)), and the Mach-reflection takes place. The Mach-stems spread along the symmetry axis (Fig. 3 ( $t=0.397$  ms)). The right-spread Mach-stem catches up with the elliptical right-spread shock wave induced by the flame, and the left-spread Mach-stem reflects at the arc wall (Fig. 3 ( $t=0.405$  ms)). Because of the interaction of the complex shock and the high-speed flame, a number of hot spots with high temperature and high pressure appear (Fig. 3 ( $t=0.425$  ms)) between the shock wave and the flame surface, which rapidly enlarge and form an over-drive detonation wave declining to stable detonation (Fig. 3 ( $t=0.449$  ms)).

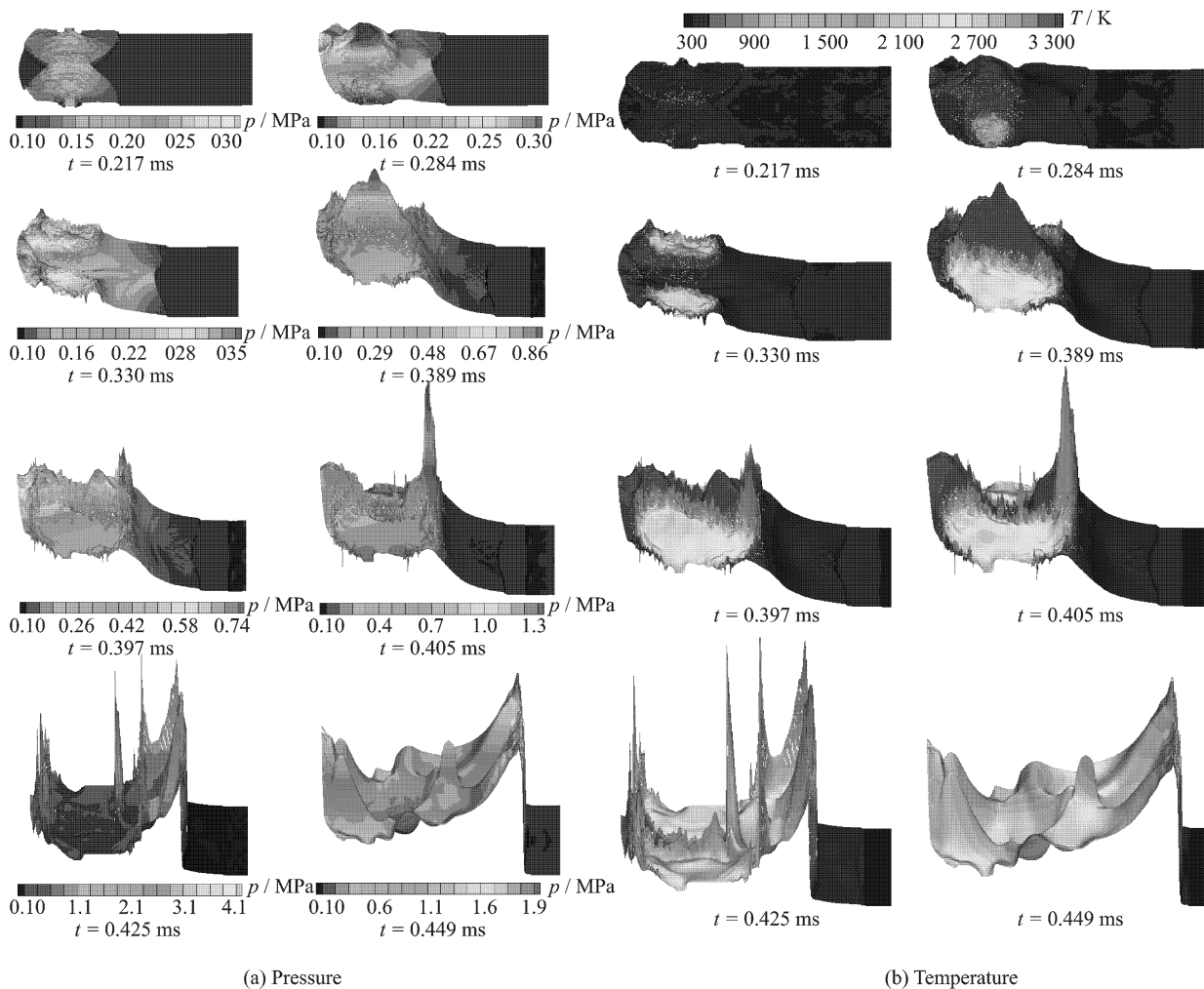


Fig. 3 Pressure and temperature distributions at different time in model (b)

In the model (c) in Fig. 1, complex shocks reflect on the right side arc wall, which strengthen and simultaneously accelerate the right-spread flame. Under the restriction of the right side arc wall, the flame accelerates convergence to the axis (Figs. 4 (a, b) ( $t$  is from 0.510 ms to 0.518 ms)), and an over-drive detonation directly happens at the axis (Fig. 4 ( $t = 0.531$  ms)). Then the strong detonation propagates along the axis to both sides. The left-spread detonation detonates the combustible mixture (Fig. 4 ( $t = 0.536$  ms)), encounters the arc wall, reflects and declines to the strong shock wave in the combustion products. The right-spread detonation detonates the combustible mixture and weakens to stable deto-

nation.

Fig. 5 is the distributions of the average pressure and velocity of post-detonation product at different locations in the rounded detonative chamber. The stable detonation forms at  $x = 300$  mm. The pressure peaks at different locations are around 1.64 MPa, the velocities of post-detonation product are 880 m/s, and the pressures of post-detonation are 0.61 MPa. The detonation velocity is 1 990 m/s, which is calculated according to the distance swept by the detonation wave in a certain time interval. The errors of these variables are less than 4% compared with the STANJAN (a chemical equilibrium solver, deve-

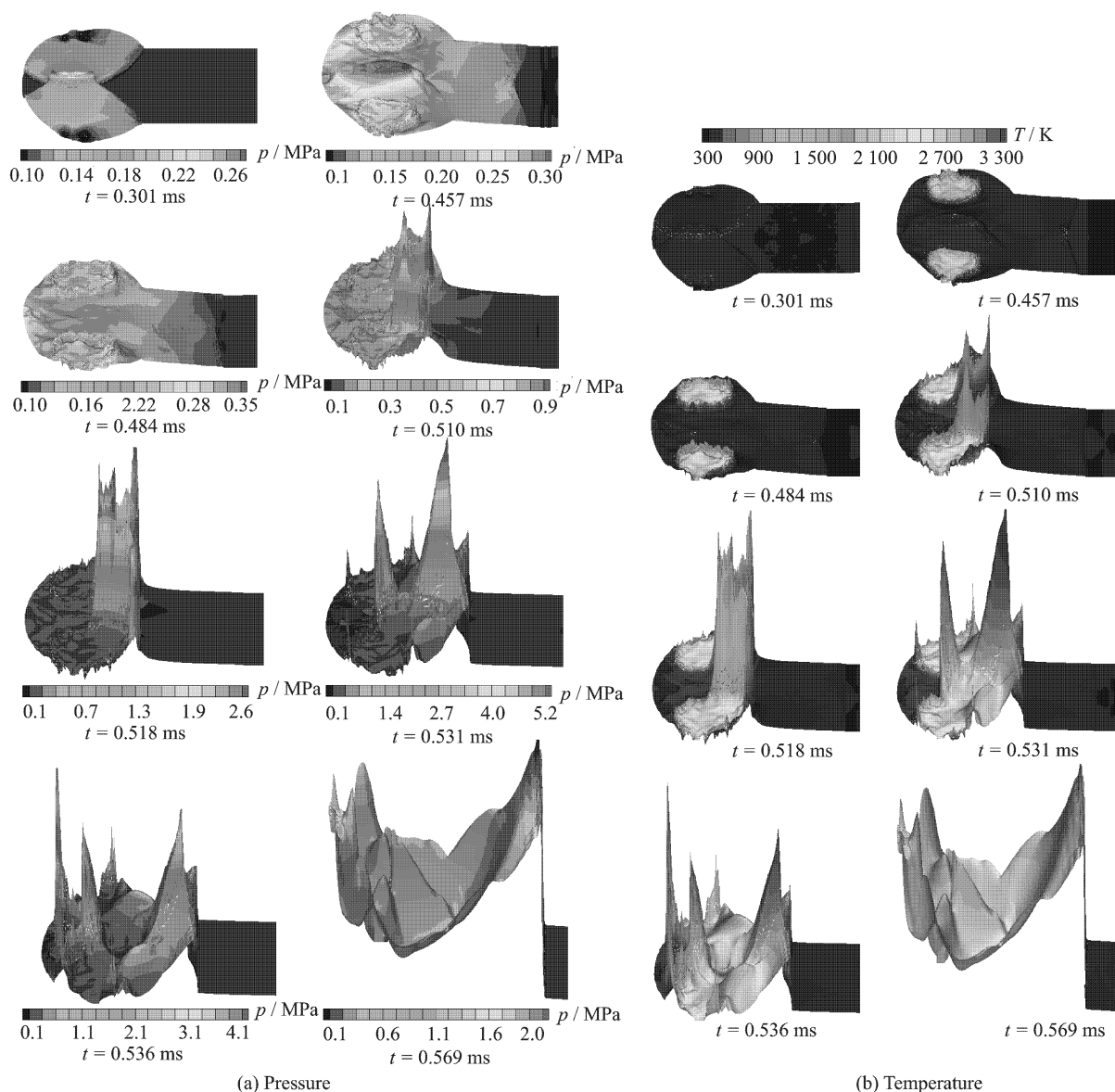


Fig. 4 Pressure and temperature distributions at different time in model (c)

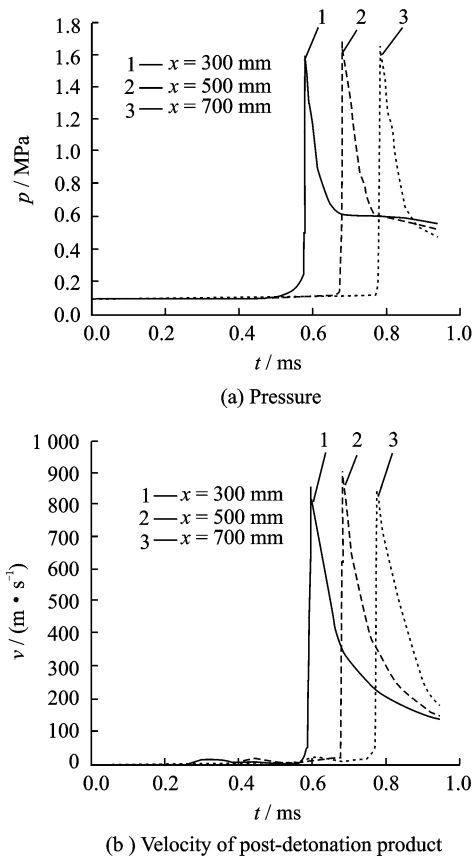


Fig. 5 Distributions of pressure and velocity of post-detonation product at different locations

veloped by Department of Mechanical Engineering Stanford University in America) values under the same conditions, which implies that the simulation is reasonable.

### 2.3 Effect of location of jet flame burner to initiation distance

The distance from the jet flame burner centre to the left arc wall ( $l$ ) affects the development of flame implosion. The distances between the detonation initiation and the steady detonation are varied by changing  $l$  from 27 mm to 75 mm in the models (b, c), as shown in Fig. 6. When the  $l$  value is large, the reflection focusing shock wave declines after passing through the long burnt zone and encountering the second collision reflection shock wave. The second collision reflection shock wave is weak if the  $l$  value is small. These conditions are not preferable, therefore, there is an optimum  $l$  value when the reflection focusing shock wave and the second collision reflection shock

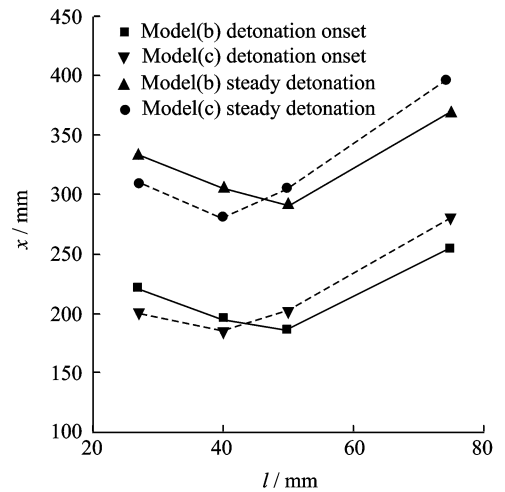


Fig. 6 Detonation distance of different jet flame burner location

wave are both strong enough to accelerate the flame.

### 2.4 Detonation initiation with multi-jet flame burners

Simulations on detonation initiation with multi-jet flame burner are carried out and the jet flame burners are set side by side along the axis. Multi-flame from jet flame burners gathers and the induced shock wave focuses, then the focusing shock wave accelerates the gathering flame. The combustible mixture in shock wave focusing cavity rapidly burns at a large scale. The shock wave collides at the axis, and the Mach-reflection takes place. The left-spread Mach-stem reflects at the arc wall and need pass through the long burnt zone to reach the chemistry reaction zone, which makes it not strong enough to accelerate the right-spread shock wave and the flame. Generally speaking, only the jet flame burner at the right side has an effect to the detonation initiation.

### 2.5 Torus-shaped jet flame and annular-planar shock wave

Simulations on the model (d) in Fig. 1 are performed to study the Torus-shaped jet flame implosion and the annular-planar shock wave focusing. The numerical results show that the torus-shaped jet flame and the induced shock

wave propagate to the shock wave focusing cavity and the rounded detonative chamber at different speeds. The shock wave concentrates at the axis and reflects on the arc wall, then forms a complex shock (Fig. 7). The flame propagates and accelerates to the right along the axis under the restrictions of the arc wall and the axis (Fig. 8). Because of the interaction among the high speed flame, the induced shock wave and the complex shock, the hot spots with high temperature and pressure appear and the initiate detonation in the combustible mixture declines to stable detonation gradually. This kind of structure can be further developed, i. e., turning the torus-shaped jet flame burner to the structure of spiral channel. The flame accelerates in the small spiral channel, which leads to the phenomena that the high speed annular flame and the strong shock wave appear, and even the further detonation may occur at the exit of spiral channel to detonate the combustible mixture in the main detonative chamber.

### 3 CONCLUSION

This paper carries out some computational simulations on structurally different detonation generator to study the phenomena, the mechanism and gas dynamics characteristics of the flame implosion and shock wave focusing. In the model (a), the direct ignition at a certain distance from thrust wall generates flame. The phenomenon of the flame implosion is analyzed. Computational studies on models (b, c) show that the laminar flame appears with low energy ignition in the ring-like jet flame burner. The laminar flame accelerates in the narrow channels, and the impingement of jet flame on the axis strengthens the shock wave to enhance the flame acceleration. Because of the function of multiple shock waves and flame, a number of hot spots appear between the shock wave and the flame surface, which rapidly enlarges and forms an over-drive detonation wave with high pressure, and then declines to the stable detonation. The distance from the jet flame

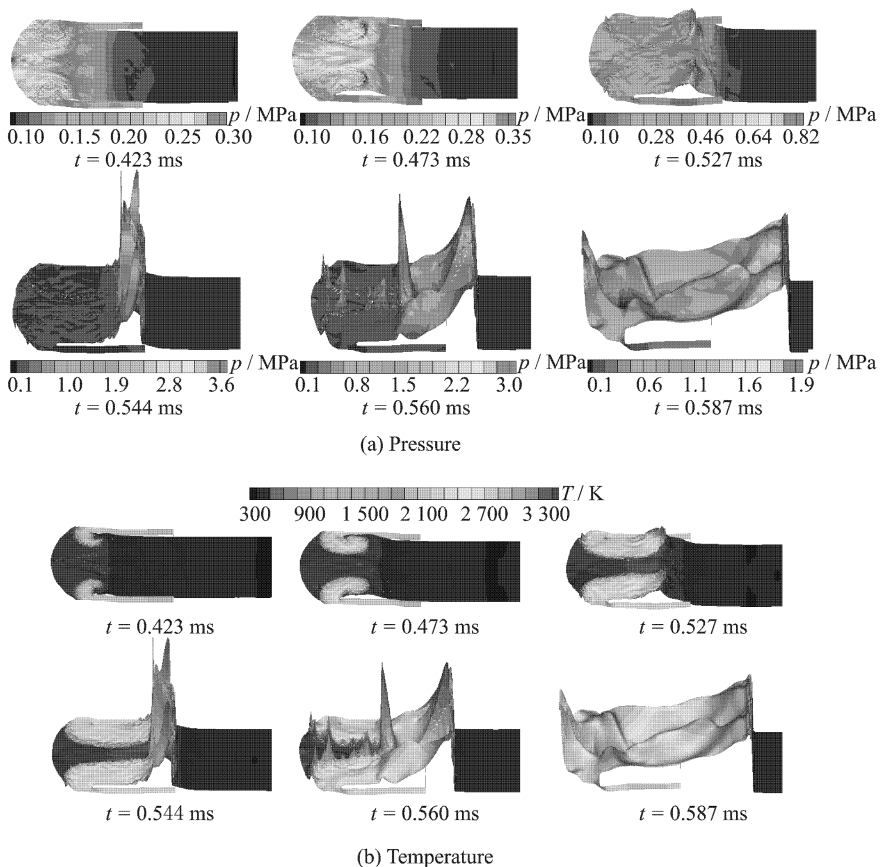


Fig. 7 Pressure and temperature distributions at different time in model (d)

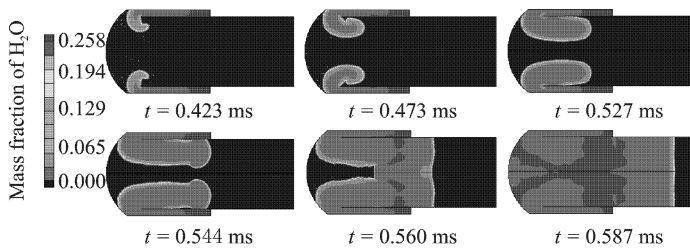


Fig. 8 Mass fraction of  $H_2O$  at different time

burner centre to the left arc wall ( $l$ ) affects the development of detonation, and there is an optimum  $l$  value when the reflection focusing shock wave and the second collision reflection shock wave are strong enough to accelerate the flame. In the model (d), the annular-planar shock wave and the flame impinge on the axis, then concentrate, reflect, and form hot spots in the focusing cavity. The hot spots detonate the reactants in the inner chamber. Through calculating and analyzing, the length of detonation initiation and stable detonation are obtained, which provide useful information for the further experimental researches. And the deep understanding on the aerodynamic characteristics and the mechanism of interaction between the flame implosion and the shock wave focusing are obtained.

## References:

[1] Levin V A, Nechaev J N, Tarasov A I. A new approach to organizing operation cycles in pulse deto-

nation engines [C]//High-Speed Deflagration and Detonation: Fundamentals and Control. Moscow: [s. n.], 2001:223-238.

[2] Bartenev I A M, Khomik I S V, Gelfand I B E. Effect of reflection type on detonation initiation at shock-wave focusing[J]. Shock Waves, 2000, 10(3):205-215.

[3] Witt B D, Ciccarelli G, Zhang F, et al. Shock reflection detonation initiation studies for pulse detonation engines[R]. AIAA 2004-3747, 2004.

[4] Thomas G O, Ward S M, Williams R L, et al. On critical conditions for detonation initiation by shock reflection from obstacles[J]. Shock Waves, 2002, 12(2):111-119.

[5] Li Chiping, Kailasanath K. Detonation initiation in pulse detonation engines [R]. AIAA 2003-1170, 2003.

[6] Jackson S I, Shepherd J E. Detonation initiation via imploding shock waves [R]. AIAA 2004-3919, 2004.

[7] Yungster S, Perkins H D. Multiple-cycle simulation of a pulse detonation engine ejector [R]. AIAA 2002-3630, 2002.

## 由火焰聚心和激波聚焦诱导的爆震波研究

秦亚欣 于军力 高歌

(北京航空航天大学航空发动机气动热力科技重点实验室,北京,100191,中国)

**摘要:**通过对几种不同结构形式的爆震发生器进行数值模拟,研究了激波聚焦和火焰聚心现象、气动特性及其机理。数值计算采用多组分理想气体详细的化学反应机理、二维轴对称非定常流动 Navier-Stokes 方程来模拟流体动力学和化学动力学过程。数值计算表明用较低的点火能量对射流火焰燃烧器中可燃混合物点火,层流火焰在狭窄管壁作用下加速,射流火焰在轴线上汇聚过程有利于激波的加强,强激波加速火焰,在多重激波与火焰反复作用下,激波和火

焰面之间出现热点,热点迅速放大并形成压力很高的过驱爆震波,而后衰减为稳定的爆震波,不同的激波聚焦腔爆震波的形成过程不同。通过对数值计算的结果进行分析,得到了起爆距离和稳定爆震距离,为进一步试验提供参考。

**关键词:**爆震波;激波聚焦;聚心火焰;爆燃向爆震的转变  
**中图分类号:**V231.2